Light Nuclei Femtoscopy and Baryon Interactions in 3 GeV Au+Au Collisions at RHIC

The STAR Collaboration

We report the measurements of proton-deuteron (p-d) and deuteron-deuteron (d-d) correlation functions in Au+Au collisions at $\sqrt{s_{\mathrm{NN}}} = 3$ GeV using fixed-target mode with the STAR experiment at the Relativistic Heavy-Ion Collider (RHIC). For the first time, the source size (R_G), scattering length (f_0), and effective range (d_0) are extracted from the measured correlation functions with a simultaneous fit. The spin-averaged f_0 for p-d and d-d interactions are determined to be -5.28 $\pm$ 0.11(stat.) $\pm$ 0.82(syst.) fm and -2.62 $\pm$ 0.02(stat.) $\pm$ 0.24(syst.) fm, respectively. The measured p-d interaction is consistent with theoretical calculations and low-energy scattering experiment results, demonstrating the feasibility of extracting interaction parameters using the femtoscopy technique. The reasonable agreement between the experimental data and the calculations from the transport model indicates that deuteron production in these collisions is primarily governed by nucleon coalescence.

Unveiling the interactions between baryons plays a fundamental role in understanding the strong interaction. In heavy-ion collisions, the measurements of two-particle femtoscopic correlations have proven to be a powerful tool for gaining insights into the space-time geometry of the particle emitting sources, as well as the interactions between pairs of particles [1–5]. Experimental efforts have been devoted to studying the strong interactions between particles measured in heavy-ion collisions at RHIC and LHC energies [5–7]. However, a majority of the studies have primarily focused on the interactions between light and strange hadrons, such as p-p [8], $\bar{p}$-$\bar{p}$ [6], p-ϕ [9], K^--p [10], p-Λ [8, 11, 12], p-Ξ [5], p-Ω [5, 13], and Λ-Λ [8, 14] pairs. Light nuclei, such as the deuteron, consist of loosely bound nucleons with binding energies on the order of several MeV. Conducting femtoscopic measurements between pairs of particles involving light nuclei, such as p-d and d-d, has significant relevance for the investigation of few-nucleon systems. These systems serve as crucial testing grounds for three-body nuclear forces, which are essential for understanding the properties of the hot and dense medium formed in heavy-ion collisions and the intrinsic structures of neutron stars [7, 15–17].

The production of light nuclei in heavy-ion collisions has been extensively explored both experimentally [3, 18–24] and theoretically [25–28]. The statistical thermal model [29, 30] and nucleon coalescence [31–33] are the two most popular models proposed to explain their production in heavy-ion collisions. Femtoscopic correlations, which provide information about the spatial distribution of particle emissions, are particularly sensitive to the emitting source. Therefore, by analyzing the femtoscopic correlations of light nuclei, we can also gain further insight into the nature of their production mechanisms.

In this letter, we report the femtoscopic measurement of two-particle correlation functions of light nuclei pairs, p-d and d-d, in Au+Au collisions at $\sqrt{s_{\mathrm{NN}}} = 3$ GeV. The data was recorded by the Solenoidal Tracker at RHIC (STAR) under the fixed-target (FXT) configuration in the year 2018. A beam of gold nuclei of energy 3.85 GeV/u was incident on a gold target of thickness 0.25 mm, corresponding to 1% of an interaction length. The target was installed inside the vacuum pipe, 2 cm below the center of the normal beam axis, and located 200.7 cm to the west of the center of the STAR detector. The minimum bias (MB) trigger condition was provided by simultaneous signals from the Beam-Beam Counters (BBC) [34] and the Time of Flight (TOF) detector [35]. To remove collisions between the beam and beam pipe, the reconstructed collision vertex position along the beam direction, V_z, is required to be within $\pm$ 2 cm and the primary vertex position in the radial plane, V_r, is required to be located within $\pm$ 1.5 cm from the center of the Au target. In total, approximately 2.6×10^8 events pass the selection criteria and are used in this analysis. The centrality of collisions is characterized by Glauber model [36, 37] fitting of the charged tracks measured in the Time Projection Chamber (TPC) [38] within the pseudo-rapidity (η) region $-2 < \eta < 0$. Further details about the experimental setup are given in Ref.[39]. The 0-60% central events are used in this analysis.

Charged-track trajectories are reconstructed from the measured space points information in the TPC. In order to select the primary tracks, each track is required to have a distance of closest approach (DCA) to the event vertex of less than 3 cm. To ensure the quality of reconstructed tracks, each track is required to have at least 15 measured points in the TPC and to have at least 52% of the possible maximum possible points for its particular geometry. The charged-particle identification is accomplished using the specific energy loss dE/dx measured in the TPC and the reconstructed rigidity. Figure 1 (a) shows the energy loss dE/dx distribution of protons and deuterons as a function of rigidity. For momentum less than 2 GeV/c, the proton and deuteron bands are sufficiently separated that particle identification (PID) can be done cleanly using only the TPC. In order to improve purity for momentum above 2 GeV/c, an additional mass-squared cut is performed using PID information from the TOF. Figure 1 (b) shows m^2/q^2 versus momentum with TOF PID.
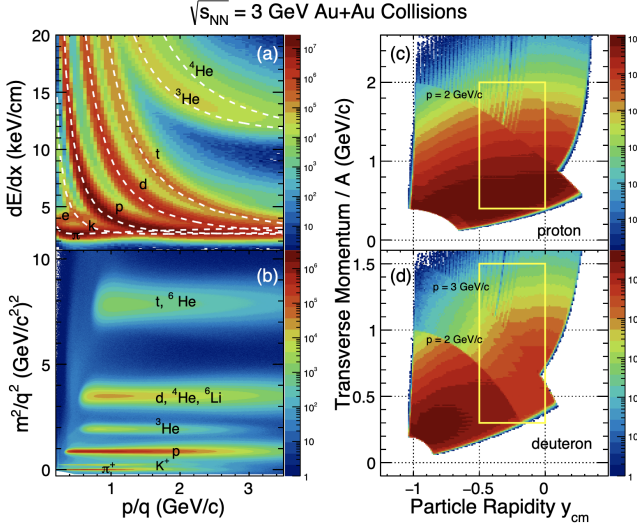
FIG. 1. (a) The $\langle dE/dx \rangle$ of charged tracks versus particle rigidity in Au+Au collisions at $\sqrt{s_{NN}} = 3\,\text{GeV}$. The dashed lines are Bichsel theoretical curves for the corresponding particle species as labeled. (b) Particle m^2/q^2 versus rigidity. The bands correspond to π^+, K^+, p, d, t, ^{3}He and ^{4}He as labeled. ^{4}He and ^{6}Li have the same m^2/q^2 as d and ^{6}He has the same m^2/q^2 as t. (c) and (d) The atomic mass number normalized transverse momentum (p_T/A) versus rapidity in the center-of-momentum frame (y_{cm}) acceptances for p and d. The bands in the distributions are caused by the momentum dependent requirements of the PID. The yellow boxes represent the selected phase space for correlation function calculation. Target rapidity is at $y_{cm} = -1.05$.

Figures 1 (c) and (d) show the momentum-space acceptance of selected protons and deuterons as a function of p_T and rapidity (y_{cm}) in the center-of-mass frame. The target is at $y_{cm} = -1.05$ and the sign of y_{cm} is chosen such that the beam travels in the positive y_{cm} direction. The $p_T - y_{cm}$ acceptance windows used for this analysis are indicated in Figure 1 (c,d).

The method used to investigate the p-d and d-d interaction relies on the particle pair correlations measured as a function of k^*, defined as the reduced relative momentum of the pair $(k^* = |\vec{p}_1 - \vec{p}_2|/2)$ in the pair rest frame, where $\vec{p}_1$ and $\vec{p}_2$ are the momenta of the particles. The experimental correlation function is defined as:

$$C_{\text{exp}}(k^*) = \mathcal{N}\frac{N_{\text{same}}(k^*)}{N_{\text{mixed}}(k^*)}, \qquad (1)$$

where $N_{\text{same}}(k^*)$ is the measured distribution of pairs with both particles coming from the same event, $N_{\text{mixed}}(k^*)$ is the reference distribution generated from mixed events, and $\mathcal{N}$ is a normalization parameter. The denominator, $N_{\text{mixed}}(k^*)$, is obtained by mixing particles from different events that have approximately the same centrality and vertex position along the z-direction. The normalization parameter $\mathcal{N}$ is chosen such that the mean value of the correlation function equals unity for $300 <$

$k^* < 500\,\text{MeV}/c$. Identical single-particle cuts are applied in both same and mixed events. The track splitting (one single particle reconstructed as two tracks) and track merging (two particles with similar momenta reconstructed as one track) effects are removed following a standard method used in STAR [40]. The efficiency and acceptance effects cancel in the $N_{\text{same}}(k^*)/N_{\text{mixed}}(k^*)$ ratio. The effect of momentum resolution on the correlation functions has been investigated using simulated tracks with known momenta, embedded into real events. More details can be found in [40]. The impact of momentum resolution on correlation functions is found to be less than 1%. The systematic uncertainties of correlation functions are obtained by varying single-particle selection criteria for protons and deuterons, feed-down contribution to protons, pair selection and normalization range. The resulting uncertainties on the correlation functions are added in quadrature.

The centrality dependence of the mid-rapidity correlation functions for p-d (top panel) and d-d (bottom panel) are displayed as a function of the relative momentum in Fig. 2. A significant suppression below unity is observed at low relative momentum of the p-d and d-d correlation functions, primarily due to the dominant repulsive Coulomb interactions. The measured correlation functions are compared to those calculated using the "Simulating Many Accelerated Strongly interaction Hadrons" (SMASH) model [41] under cascade mode. The SMASH is a newly developed hadronic transport model especially suitable for studying the dynamical evolution of heavy-ion collisions at high baryon density [41]. Key features of nuclear collision dynamics including initial condition, baryon stopping [42, 43], resonances production and detail balance are implemented in the model. The transport model offers full phase information of particles at kinetic freeze-out, recorded at the last scattering time, allowing apply experimental cuts which is specially important for realistically determination of collision centrality, the correlation analysis as well as light nuclei production [27, 44]. The particle's freeze-out phase space info is reconstructed with the last collision time provided by the model calculation [27]. Within the SMASH framework, we consider two distinct production mechanisms for deuterons. In the first approach, deuterons were produced through nucleon coalescence, with their formation probability determined by the Wigner function, which takes into account the relative momentum and spatial coordinates of protons and neutrons [45]. The second mechanism accounts for directly-produced deuterons through hadron scattering processes ($p+n+\pi \leftrightarrow d+\pi$) under default setting from SMASH. The calculations with the coalescence mechanism provide a better description of the d-d correlation functions, accurately capturing the observed correlations. In comparison, the directly-produced mechanism tends to underestimate the strength of the correlations, especially for the d-d pairs. These
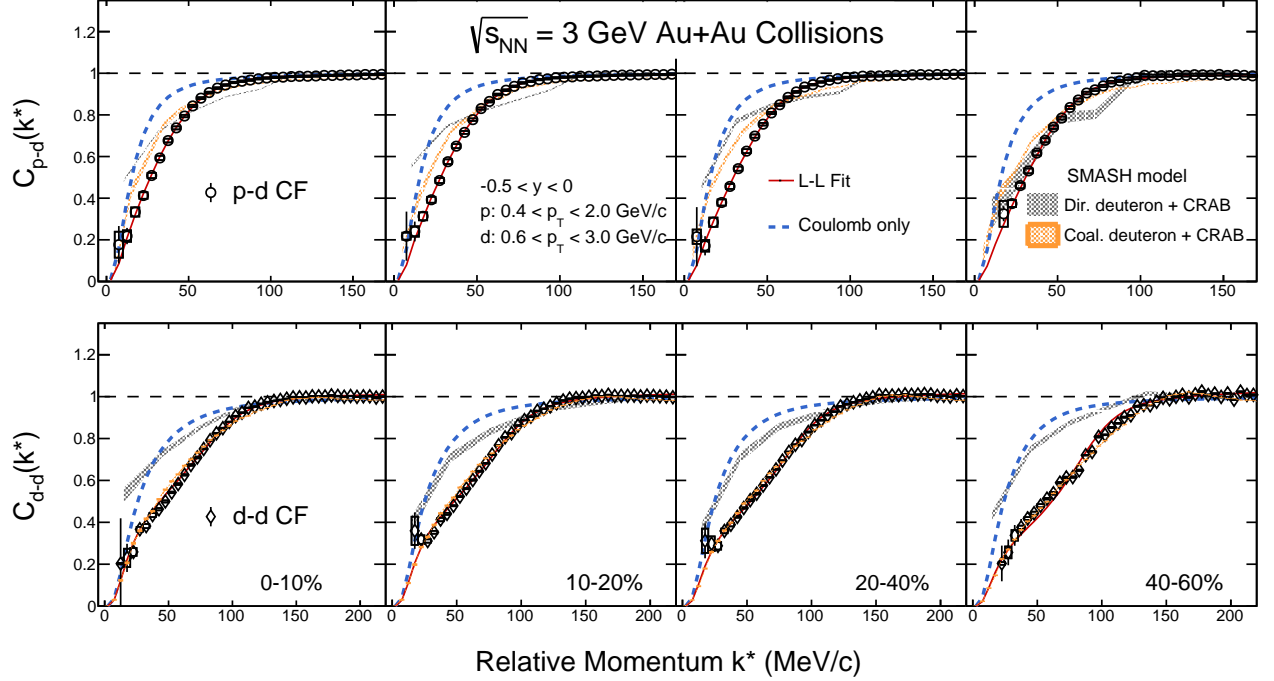
FIG. 2. Centrality dependence of the mid-rapidity correlation functions for *p-d* (top panel) and *d-d* (bottom panel) displayed as a function of the relative momenta. Statistical and systematic uncertainties from the measurements are shown as bars and boxes, respectively. The results of the Lednický-Lyuboshits (LL) fits are shown as the red-lines. Orange bands represent the calculations from the SMASH model with coalescence procedure for the formation of deuterons plus CRAB afterburner while gray bands show the model calculation with directly produced deuterons plus CRAB. Blue dashed lines are the results with Coulomb interactions only.

correlation functions provide further evidence supporting the notion that deuterons are primarily created through the coalescence mechanism, as indicated by the previous measurements of collectivity and yields of light nuclei [46, 47] in high-energy nuclear collisions. Note that the SMASH model itself does not incorporate the effect of quantum statistics or the final-state interaction (the Coulomb potential and strong interaction) after kinetic freeze-out, hence these are calculated by the "Correlation After Burner (CRAB) [48]". The strong interaction potentials for the *p-d* and *d-d* are adopted from previous studies [49].

The final-state interaction for *p-d* and *d-d* has been modeled using the Lednický-Lyuboshits (LL) approach [50, 51]. Theoretically the correlation function can be expressed as

$$C\left(k^*\right) = \int S(r) \left| \Psi\left(\overrightarrow{k^*}, \vec{r}\right) \right|^2 \, \mathrm{d}^3 r \qquad (2)$$

where r is the relative distance of the particles that make up the pair of interest. $S(r)$ is the distribution of this relative distance for particles emitted in the collision. $\Psi\left(\overrightarrow{k^*}, \vec{r}\right)$ represents the wavefunction of the relative motion for the pair of interest. In this approach, the forward scattering amplitude including Coulomb interaction can be represented as:

$$f_c^S\left(k^*\right) = \left[\frac{1}{f_0^S} + \frac{1}{2}d_0^S k^{*2} - \frac{2}{a_c}h(\eta) - ik^* A_c(\eta)\right]^{-1} \quad (3)$$

where a_c is the Bohr radius for particle pairs, $\eta = (k^* a_c)^{-1}$,

$$h(\eta) = \eta^2 \sum_{n=1}^{\infty} \left[n(n^2 + \eta^2)\right]^{-1} - C - \ln|\eta|$$

(here $C = 0.5772$ is the Euler constant), $A_c(\eta) = 2\pi\eta(e^{2\pi\eta} - 1)^{-1}$ is the Coulomb penetration factor, f_0^S is the scattering length and d_0^S is the effective range for a given total spin S. For *p-d* interactions, two possible spin configurations are considered, $S = 1/2$ and $S = 3/2$, for a doublet and quartet state, respectively. For *d-d* interactions, one considers $S = 0$ and $S = 2$, for a singlet and quintet state. To make the f_c symmetric respect to identical fermions system, the $S = 1$, triplet state in the *d-d* system is not taken into account because it is not relevant to s-wave. The different spin configurations can not be distinguished in these measurements, so spin-averaged results are presented. Throughout this paper the standard sign convention is adopted, where, a positive f_0 indicates an attractive interaction in a baryon-baryon system, and

a negative sign represents a repulsive potential or the presence of a bound state. More detailed discussions about the LL approach can be found in Refs. [6, 50, 51]. Note the following caveats: (i) The size of deuteron is not considered in our treatment, in other words, the deuteron is treated as a point-like particle; and (ii) the LL model relies on the smoothness assumption [52]. These effects may become significant in small systems, such as p+p collisions [7]. However, the relatively large source size observed in heavy-ion collisions justifies the application of the LL approach [50].
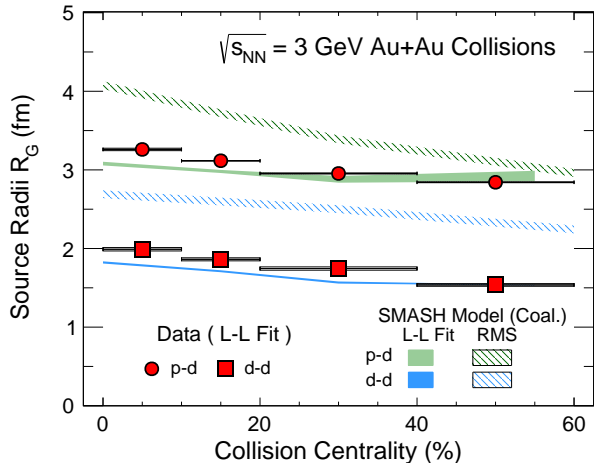
FIG. 3. Collision centrality dependence of the source radius parameter extracted from p-d (circles) and d-d (squares) correlation functions in $\sqrt{s_{NN}} = 3\,\text{GeV}$ Au+Au collisions. Statistical and systematic uncertainties are all smaller than the size of the symbols. The values of the Gaussian source radius from SMASH model are shown as green and blue bands, for p-d and d-d pairs, respectively. The shadow bands represent the RMS values calculated from SMASH model.

The source radius and interaction parameters are extracted by fitting the p-d and d-d correlation functions with LL model using the range $k^* < 200$ MeV/c. The fitting is performed simultaneously to the data in four centrality bins using four source radii (one R_G^{data} for each centrality) and common strong interaction parameters f_0 and d_0. To evaluate the systematic uncertainties associated with the fitting procedure, different fitting ranges are considered. The obtained R_G^{data}, for the p-d and d-d pairs in different centralities from the LL fit are presented in Figure 3. It is observed that the R_G of both p-d and d-d pairs exhibit a monotonic decrease from central to peripheral collisions. Additionally, the R_G^{data} of p-d is consistently larger than that of d-d in all centrality classes. Based on the observation of m_T-scaling [39, 53, 54], the overall larger $\langle m_T \rangle$ of d-d pairs (2.05 ± 0.01 GeV/c) compared to that of the p-d pairs (1.57 ± 0.01 GeV/c) might explain the observed difference in source radii. A similar phenomenon in p-d and d-d correlation analyses was
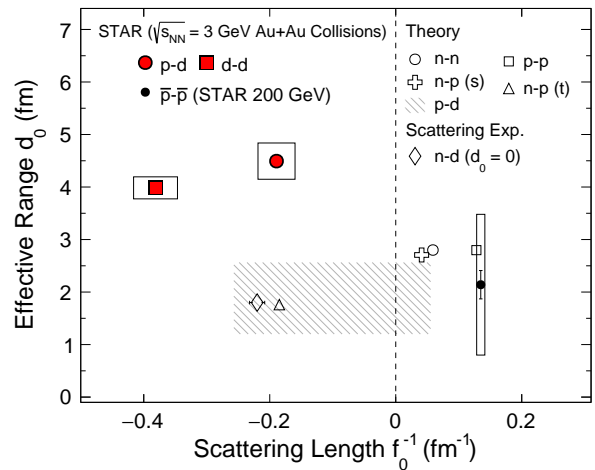

FIG. 4. Spin-averaged final state strong interaction parameters: f_0 scattering length, and d_0 effective range, extracted from p-d (filled circle) and d-d (filled square) correlation functions. The statistical uncertainties are smaller than the marker size. Open boxes represent the systematic uncertainties. Data of $\bar{p}$-$\bar{p}$ correlation function in 200 GeV Au+Au collisions [6] are shown as the solid black point. The interaction parameters from n-n, p-p, n-p singlet (s), n-p triplet (t) states [59, 60], n-d [61, 62] and p-d [63–67] are shown as open symbols and hatched area.

also observed in ^{40}Ar+^{58}Ni collisions at 77 MeV/u [55]. The model calculations using coalescence plus CRAB for both p-d and d-d pair correlation functions are compatible with the experimental data (as shown in Figure 2), the resulting radii R_G^{SMASH} using same LL fit closely match the data. As one can see in Figure 3, the root mean square (RMS) values of the source radii directly extracted from SMASH model calculation are larger than the static source radii obtained under the Gaussian assumption. The difference between RMS and R_G can be attributed to the dynamical expansion of the system in nuclear collisions [56–58]. The resulting source has a time distribution in the model calculation. This leads to a tail in the distance distribution, which in turn cannot be described by a simple Gaussian distribution, making the value of R_G smaller than that of the RMS value.

The extracted spin-averaged scattering length f_0 and effective range d_0 obtained from the model fit are shown in Figure 4. The strong interaction parameters are assumed to be independent of centrality, enabling a simultaneous fit across all centrality bins to extract f_0 and d_0. For comparison, the interaction parameters for n-p, p-p, n-p singlet and triplet states [59, 60] as well as $\bar{p} - \bar{p}$ measured by STAR [6] are also shown in Fig. 4. In contrast to the data obtained from $\bar{p}$-$\bar{p}$ correlations and the majority of model predictions for nucleon-nucleon interactions, it is remarkable that the spin-averaged f_0 is negative for both p-d and d-d interaction. This observa-

tion is consistent with the combination of the repulsive interactions in quartet (quintet) spin state for p-d (d-d) along with the presence of bound states (^{3}He for p-d and ^{4}He for d-d). Remarkably, the measured f_0 of p-d interactions from the femtoscopy method is consistent with n-d interaction parameters from theory calculation [61] and low-energy scattering experiment measurement [62]. This supports the feasibility of extracting interaction parameters with the two-particle correlation technique. Recently the ALICE experiment reported a new measurement on the p-d correlation function from 13 TeV p+p collisions [7]. In contrast to the heavy-ion results presented here, that analysis indicates that a three-body interaction [68] seems to be required in order to reproduce the measured p-d correlation function in the elementary collisions. The d-d correlation functions presented here are the first such experimental results from high-energy nuclear collisions.

In summary, we have reported the measurements of the mid-rapidity light nuclei correlation functions for p-d and d-d pairs in Au+Au collisions at $\sqrt{s_{\mathrm{NN}}} = 3\,\mathrm{GeV}$ measured by the STAR experiment at RHIC. The measured correlation functions are reasonably described by the transport model SMASH with afterburner calculations. The extracted Gaussian equivalent static source radii, R_G^{data}, display a decreasing trend from central to peripheral collisions. Larger values of the radii are observed from the p-d pairs compared to those of d-d pairs in all centrality bins. The values of the fitted R_G^{data} are found to be consistently smaller than the RMS values extracted from the model calculations implying time-dependent expansion. For the first time, the strong interaction parameters of p-d and d-d pairs are extracted from heavy-ion collisions. The extracted scattering lengths (spin-averaged), f_0, are found to be consistent with the bound-state of light nuclei (^{3}He and ^{4}He), respectively. Within uncertainties, the measured parameters for the p-d interaction are consistent with results of low-energy scattering experiment and model calculations [63–67]. In addition, results imply that coalescence is the dominant process for deuteron formation in the high-energy nuclear collisions. These systematic measurements of correlation functions and interaction parameters provide valuable insights into the production mechanism of light nuclei and many-body interactions.

[1] R. Lednicky, Nucl. Phys. A **774**, 189 (2006), arXiv:nucl-th/0510020.
[2] F.-q. Wang and S. Pratt, Phys. Rev. Lett. **83**, 3138 (1999), arXiv:nucl-th/9907019.
[3] J. Chen et al., (2024), arXiv:2407.02935 [nucl-ex].
[4] L. Adamczyk et al. (STAR), Phys. Rev. C **92**, 014904 (2015), arXiv:1403.4972 [nucl-ex].
[5] A. Collaboration et al. (ALICE), Nature **588**, 232 (2020), [Erratum: Nature 590, E13 (2021)], arXiv:2005.11495 [nucl-ex].
[6] L. Adamczyk et al. (STAR), Nature **527**, 345 (2015), arXiv:1507.07158 [nucl-ex].
[7] S. Acharya et al. (ALICE), Phys. Rev. X **14**, 031051 (2024), arXiv:2308.16120 [nucl-ex].
[8] S. Acharya et al. (ALICE), Phys. Rev. C **99**, 024001 (2019), arXiv:1805.12455 [nucl-ex].
[9] S. Acharya et al. (ALICE), Phys. Rev. Lett. **127**, 172301 (2021), arXiv:2105.05578 [nucl-ex].
[10] S. Acharya et al. (ALICE), Phys. Rev. Lett. **124**, 092301 (2020), arXiv:1905.13470 [nucl-ex].
[11] J. Adams et al. (STAR), Phys. Rev. C **74**, 064906 (2006), arXiv:nucl-ex/0511003.
[12] S. Acharya et al. (ALICE), Phys. Lett. B **833**, 137272 (2022), arXiv:2104.04427 [nucl-ex].
[13] J. Adam et al. (STAR), Phys. Lett. B **790**, 490 (2019), arXiv:1808.02511 [hep-ex].
[14] L. Adamczyk et al. (STAR), Phys. Rev. Lett. **114**, 022301 (2015), arXiv:1408.4360 [nucl-ex].
[15] D. Gerstung, N. Kaiser, and W. Weise, Eur. Phys. J. A **56**, 175 (2020), arXiv:2001.10563 [nucl-th].
[16] D. Lonardoni, A. Lovato, S. Gandolfi, and F. Pederiva, Phys. Rev. Lett. **114**, 092301 (2015), arXiv:1407.4448 [nucl-th].
[17] K. Hebeler, J. D. Holt, J. Menendez, and A. Schwenk, Ann. Rev. Nucl. Part. Sci. **65**, 457 (2015), arXiv:1508.06893 [nucl-th].
[18] J. Adam et al. (ALICE), Phys. Rev. C **93**, 024917 (2016), arXiv:1506.08951 [nucl-ex].
[19] L. Adamczyk et al. (STAR), Phys. Rev. C **94**, 034908 (2016), arXiv:1601.07052 [nucl-ex].

[20] S. Acharya *et al.* (ALICE), Phys. Rev. C **97**, 024615 (2018), arXiv:1709.08522 [nucl-ex].

[21] J. Adam *et al.* (STAR), Phys. Rev. C **99**, 064905 (2019), arXiv:1903.11778 [nucl-ex].

[22] M. Abdulhamid *et al.* (STAR), Phys. Rev. Lett. **130**, 202301 (2023), arXiv:2209.08058 [nucl-ex].

[23] S. Acharya *et al.* (ALICE), Phys. Rev. C **107**, 064904 (2023), arXiv:2211.14015 [nucl-ex].

[24] STAR, (2023), arXiv:2311.11020 [nucl-ex].

[25] X.-Y. Zhao, Y.-T. Feng, F.-L. Shao, R.-Q. Wang, and J. Song, Phys. Rev. C **105**, 054908 (2022), arXiv:2201.10354 [hep-ph].

[26] S. Gläßel, V. Kireyeu, V. Voronyuk, J. Aichelin, C. Blume, E. Bratkovskaya, G. Coci, V. Kolesnikov, and M. Winn, Phys. Rev. C **105**, 014908 (2022), arXiv:2106.14839 [nucl-th].

[27] J. Staudenmaier, D. Oliinychenko, J. M. Torres-Rincon, and H. Elfner (SMASH), Phys. Rev. C **104**, 034908 (2021), arXiv:2106.14287 [hep-ph].

[28] W. Zhao, C. Shen, C. M. Ko, Q. Liu, and H. Song, Phys. Rev. C **102**, 044912 (2020), arXiv:2009.06959 [nucl-th].

[29] T. R. Halemane and A. Z. Mekjian, Phys. Rev. C **25**, 2398 (1982).

[30] A. Andronic, P. Braun-Munzinger, J. Stachel, and H. Stocker, Phys. Lett. B **697**, 203 (2011), arXiv:1010.2995 [nucl-th].

[31] L. P. Csernai and J. I. Kapusta, Phys. Rept. **131**, 223 (1986).

[32] Y. Oh, Z.-W. Lin, and C. M. Ko, Phys. Rev. C **80**, 064902 (2009), arXiv:0910.1977 [nucl-th].

[33] H. Sato and K. Yazaki, Phys. Lett. B **98**, 153 (1981).

[34] F. S. Bieser *et al.*, Nucl. Instrum. Meth. A **499**, 766 (2003).

[35] M. Anderson *et al.*, Nucl. Instrum. Meth. A **499**, 659 (2003), arXiv:nucl-ex/0301015.

[36] R. L. Ray and M. Daugherity, J. Phys. G **35**, 125106 (2008), arXiv:nucl-ex/0702039.

[37] M. L. Miller, K. Reygers, S. J. Sanders, and P. Steinberg, Ann. Rev. Nucl. Part. Sci. **57**, 205 (2007), arXiv:nucl-ex/0701025.

[38] M. Anderson *et al.*, (2003), 10.1016/s0168-9002(02)01964-2.

[39] J. Adam *et al.* (STAR), Phys. Rev. C **103**, 034908 (2021), arXiv:2007.14005 [nucl-ex].

[40] J. Adams *et al.* (STAR), Phys. Rev. C **71**, 044906 (2005), arXiv:nucl-ex/0411036.

[41] J. Weil *et al.*, Phys. Rev. C **94**, 054905 (2016), arXiv:1606.06642 [nucl-th].

[42] A. Schäfer, I. Karpenko, X.-Y. Wu, J. Hammelmann, and H. Elfner (SMASH), Eur. Phys. J. A **58**, 230 (2022), arXiv:2112.08724 [hep-ph].

[43] J. Mohs, S. Ryu, and H. Elfner (SMASH), J. Phys. G **47**, 065101 (2020), arXiv:1909.05586 [nucl-th].

[44] J. Mohs, M. Ege, H. Elfner, and M. Mayer (SMASH), Phys. Rev. C **105**, 034906 (2022), arXiv:2012.11454 [nucl-th].

[45] W. Zhao, L. Zhu, H. Zheng, C. M. Ko, and H. Song, Phys. Rev. C **98**, 054905 (2018), arXiv:1807.02813 [nucl-th].

[46] M. S. Abdallah *et al.* (STAR), Phys. Lett. B **827**, 136941 (2022), arXiv:2112.04066 [nucl-ex].

[47] M. I. Abdulhamid *et al.* (STAR Collaboration), Phys. Rev. Lett. **130**, 202301 (2023).

[48] https://web.pa.msu.edu/people/pratts/freecodes/crab.

[49] B. K. Jennings, D. H. Boal, and J. C. Shillcock, Phys. Rev. C **33**, 1303 (1986).

[50] R. Lednicky and V. L. Lyuboshits, Yad. Fiz. **35**, 1316 (1981).

[51] K. Morita, S. Gongyo, T. Hatsuda, T. Hyodo, Y. Kamiya, and A. Ohnishi, Phys. Rev. C **101**, 015201 (2020), arXiv:1908.05414 [nucl-th].

[52] M. A. Lisa, S. Pratt, R. Soltz, and U. Wiedemann, Ann. Rev. Nucl. Part. Sci. **55**, 357 (2005), arXiv:nucl-ex/0505014.

[53] S. Acharya *et al.* (ALICE), Phys. Lett. B **811**, 135849 (2020), arXiv:2004.08018 [nucl-ex].

[54] J. Adam *et al.* (ALICE), Phys. Rev. C **92**, 054908 (2015), arXiv:1506.07884 [nucl-ex].

[55] K. Wosinska *et al.*, Eur. Phys. J. A **32**, 55 (2007).

[56] M. S. Abdallah *et al.* (STAR), Phys. Lett. B **827**, 137003 (2022), arXiv:2108.00908 [nucl-ex].

[57] J. Adams *et al.* (STAR), Nucl. Phys. A **757**, 102 (2005), arXiv:nucl-ex/0501009.

[58] Q. Li, M. Bleicher, and H. Stocker, Phys. Lett. B **663**, 395 (2008), arXiv:0802.3618 [nucl-th].

[59] L. Mathelitsch and B. J. Verwest, Phys. Rev. C **29**, 739 (1984).

[60] I. Šlaus, Y. Akaishi, and H. Tanaka, Phys. Rept. **173**, 257 (1989).

[61] H. Witaa, A. Nogga, H. Kamada, W. Gloeckle, J. Golak, and R. Skibinski, Phys. Rev. C **68**, 034002 (2003).

[62] D. G. Hurst and N. Z. Alcock, Phys. Rev. **80**, 117 (1950).

[63] T. C. Black, H. J. Karwowski, E. J. Ludwig, A. Kievsky, S. Rosati, and M. Viviani, Phys. Lett. B **471**, 103 (1999).

[64] E. Huttel, W. Arnold, H. Baumgart, H. Berg, and G. Clausnitzer, Nucl. Phys. A **406**, 443 (1983).

[65] W. T. H. Van Oers and K. W. Brockman, Nucl. Phys. A **92**, 561 (1967).

[66] A. Kievsky, S. Rosati, M. Viviani, C. R. Brune, H. J. Karwowski, E. J. Ludwig, and M. H. Wood, Phys. Lett. B **406**, 292 (1997), arXiv:nucl-th/9706077.

[67] J. Arvieux, Nucl. Phys. A **221**, 253 (1974).

[68] M. Viviani, S. König, A. Kievsky, L. E. Marcucci, B. Singh, and O. Vázquez Doce, (2023), arXiv:2306.02478 [nucl-th].